Multivariate Host-Pathogen Interactions Driving Heterogeneous Viral Shedding and CD8$^+$ T cell Control of Influenza Virus Infection

Nicole Bruce[1,#], Jordan J.A. Weaver[1,#], Cailan Jeynes-Smith[1], Fatemeh Beigmohammadi[3,4], Solène Hegarty-Cremer[3,4], Amanda P. Smith[1], Morgan Craig[3,4], Amber M. Smith[1,2,*]

[1]Department of Pediatrics, University of Tennessee Health Science Center, Memphis, TN USA

[2]Department of Microbiology, Immunology, and Biochemistry, University of Tennessee Health Science Center, Memphis, TN USA

[3]Sainte-Justine University Hospital Research Centre, Montréal, Québec, Canada

[4]Department of Mathematics and Statistics, Université de Montréal, Montréal, Québec, Canada

[#]Equal contribution, ordered alphabetically

*Corresponding author: Amber M Smith, amber.smith@uthsc.edu

Abstract

Influenza virus infections vary widely in severity, with human challenge studies revealing substantial heterogeneity in viral shedding and immune responses. Yet, the mechanistic basis of this variability remains unresolved. Here, we applied a multivariate mechanistic modeling framework to determine how variation in viral replication and CD8$^+$ T cell responses shapes infection kinetics and symptom dynamics in individuals experimentally challenged with H1N1 influenza virus. The analysis identified six distinct infection clusters arising from multivariate influences, including viral dose and individualized rates of viral infectivity. Baseline T cell levels contributed minimally, and model outputs suggested a tradeoff between CD8$^+$ T cell efficacy and expansion. Two participants showed evidence of reinfection despite being antibody negative, and modeling their data indicated that host–pathogen interactions remained consistent with those from primary infections, though data were insufficient to distinguish between cytotoxic and IFN-γ-mediated protection. Modeling of symptom trajectories further revealed potential subjectivity in symptom reporting, independent of viral strain. Collectively, these findings demonstrate how mechanistic modeling can improve the predictability of influenza outcomes and reveal that intrinsic human variation can converge on similar infection trajectories.

Introduction

Influenza virus infects millions each year, and the predictability of developing symptomatic infection is difficult. In addition, there is significant variability in viral shedding patterns, immune responses, and symptom presentation, with viral loads typically being a poor predictor of severity. Cellular immunity, humoral immunity, and cytokines have all been noted as statistical correlates in the risk of symptomatic influenza and in outcome[1–23], but these do not necessarily lead to strong differences in infection trajectories and may not always be causal. Recent studies have identified substantial variability in baseline immunity due to genetics, environmental exposures, comorbidities, and infection history[3,19,24–32], which can influence viral replication and the ensuing immune response. However, small differences in viral loads can be accompanied by large differences in cellular immunity[15,33–36], creating difficulty in reliably predicting infection outcome from immune data even when paired with advanced statistical approaches. This highlights the nonlinearity of immunity and the need to account for multivariate interindividual heterogeneity using mechanistic computational frameworks[37].

Cell-mediated immunity, which is central to the resolution of influenza infections, has been shown to vary significantly between individuals, where elevated $CD4^+$ and $CD8^+$ T cells have been correlated to protection from symptomatic infection[3,4,7,11,13,16,17,20,21,23]. However, higher influenza-specific T cell counts or frequencies in the blood are not typically associated with reduced viral shedding, and less is known about whether individuals with naturally higher baseline cell counts would be more protected from exposure to a novel influenza virus, such as during a pandemic. Human challenge studies provide a unique perspective on influenza infections in individuals lacking antibody-mediated immunity[18,20,38–53]. These studies control for the timing of infection, virus strain, and dose, facilitating the identification of interindividual variability in viral loads, immune responses, and symptoms due to other intrinsic factors. The data demonstrate that viral shedding, immunity, and symptoms vary widely between individuals, even in cases of mild infection, and that prior infection does not always confer protection. What drives the heterogeneity in infection dynamics remains unclear.

The complexity of immunity, influenza virus infection, and human variation complicates efforts to identify the determinants that shape individual host-pathogen trajectories and outcomes. Using a mechanistic mathematical modeling approach that accounts for multivariate and nonlinear host-pathogen interactions, we sought to define the signatures underlying variation in viral shedding and $CD8^+$ T cell responses while considering differential viral dosing, viral replication, baseline

$CD8^+$ T cell populations, and $CD8^+$ T cell functionality. The analyses revealed that interindividual heterogeneity during a primary infection can unite to create non-unique trajectories without a strong dependence on baseline T cells. It also demonstrated that symptoms are predictable but subjective and without direct correlation to systemic innate immunity. We extended the model to study suspected scenarios of reinfection, demonstrating the predictability of re-exposure events but the inability of the data to distinguish between mechanisms of IAV-specific $CD8^+$ T cell cytotoxicity and $CD8^+$ T cell-derived IFN-γ-mediated protection. Collectively, these results emphasize that individualism does not guarantee individualized outcomes and that pairing quantitative data with mechanistic modeling enhances the interpretability and predictability of influenza virus infections.

Materials and Methods

Influenza Infection, Immune, and Symptoms Following Challenge with H1N1

Cohort 1. We used data from a study where adult human volunteers (aged 18-45 y) were intranasally infected with 3.5 x 10^6 $TCID_{50}$ (250 μl; ID numbers beginning with 1), 7 x 10^6 $TCID_{50}$ (250 μl; ID numbers beginning with 2), or 7 x 10^6 $TCID_{50}$ (500 μl; ID numbers beginning with 3) influenza A/California/04/2009 (H1N1)[38]. Nasal washes were collected daily from days 1 to 7 to quantify viral loads (copies/ml), and blood was collected from -1 to 7 to quantify $CD8^+$ T cell frequencies. Of the 35 individuals in the study, 12 had more than one day of positive viral shedding (IDs 103, 107, 110, 111, 112, 204, 207, 302, 307, 308, 311, and 312; denoted here as 'Cohort 1'). Low viral measurements that occurred between two higher viral load measurements were considered a failed sample and excluded from our analysis (denoted with dashed outlined markers). The reported viral loads for some individuals (IDs 103, 110, 111, 112, 204, and 207) on days 1 and/or 2 post-infection were reported as zero despite confirmed infection. Because it is unclear if these are failed tests, below a limit of detection, or true zero measurements, we imputed the values using the geometric mean of the individuals who had robust measurements (i.e., 6.6 x 10^3 copies/ml for day 1 and 1.7 x 10^5 copies/ml for day 2; denoted as open markers). The limitations of data collection made this a preferable approach to have sufficient data for the mathematical model framework.

We used the matched $CD8^+$ T cell frequencies for activated ($CD38^+$) effector ($CD45RA^+CD27^-CCR7^-$) and memory ($CD45RA^-CD27^+$) phenotypes. We chose these phenotypes because they most closely resemble the dynamics of antigen-specific effector and memory $CD8^+$ T cells in the lung within animal studies[34]. Because total PBMC counts for each participant were not reported,

cell counts were estimated by multiplying the abundances by an arbitrary 2.6×10^7 cells for each phenotype for each individual. This was rationalized by comparing cell abundances with cell counts from murine data[34], which suggested relatively similar timescales of $CD8^+$ T cell expansion and peaks at the time when $CD8^+$ T cells are most active in clearing infected cells (**Figure S1**). However, it is a notable limitation of the data, where total cell counts may differ between individuals.

Total symptom scores were reported by the individuals on a 0-51 scale comprised of 0-3 ratings (0: absent; 1: mild; 2: moderate; 3: severe) for respiratory symptoms (breathing difficulty, cough, hoarseness, nasal stuffiness/congestion, runny nose, sneezing, sore throat, and wheezy chest) and pain (abdominal pain, diarrhea, earache, facial or eye pain/tenderness, fatigue, fever, headache, musculoskeletal ache, and nausea/vomiting).

Cohort 2. We used data from a study where 28 adult human volunteers (ages 18-40 y) were intranasally infected with 1×10^5 $TCID_{50}$ influenza A/Texas/36/91 (H1N1) and exhibited more than one day of viral shedding[39] (denoted as 'Cohort 2'). Daily viral loads ($TCID_{50}$) were quantified from nasal washes, and symptom scores were recorded by the infected individuals. Total symptom scores were reported on a 0-36 scale comprised of 0-3 ratings for breathing difficulty, fever, headache, hoarseness, fatigue, coughing, sneezing, sore throat, runny nose, earache, muscle ache, and chest pain.

Mathematical Model of Primary Influenza Infection

To describe the dynamics of influenza infection, we modified our previously validated mathematical model that describes the interactions between the virus and effector and memory $CD8^+$ T cells[34]. Briefly, healthy epithelial cells (T) become infected at rate βV per day and undergo an eclipse phase (I_1). The eclipse cells transition to productively infected cells (I_2) at rate k per day. These cells produce virus (V) at rate p per cell per day, which is then cleared at rate c per day. The infected cells (I_2) are cleared by innate mechanisms at rate δ per day and by effector $CD8^+$ T cells (E) at a density-dependent rate of $\delta_E(I_2)$. We model the effector $CD8^+$ T cell expansion phase using a linear chain trick, where activation of earlier effector cells (E_1) occurs at rate ξ per cell per day. The transition rate through each differentiation state ($E_{i+1\ldots n}$) occurs at $a = n/\tau_E$ per day, where n is the number of states and τ_E is the time delay. The terminally differentiated effector $CD8^+$ T cells (E) transition into memory $CD8^+$ T cells (E_M) at rate ζ per day after τ_M days. The model is given by Equations (1)-(8).

$$\frac{dT}{dt} = -\beta TV \tag{1}$$

$$\frac{dI_1}{dt} = \beta TV - kI_1 \tag{2}$$

$$\frac{dI_2}{dt} = kI_1 - \delta I_2 - \frac{\delta_E E I_2}{K_{\delta_E} + I_2} \tag{3}$$

$$\frac{dV}{dt} = pI_2 - cV \tag{4}$$

$$\frac{dE_1}{dt} = \xi I_2(t - \tau_I) - \frac{n}{\tau_E} E_1 \tag{5}$$

$$\frac{dE_{i+1,\ldots,n}}{dt} = \frac{n}{\tau_E}(E_i - E_{i+1}) \tag{6}$$

$$\frac{dE}{dt} = \frac{n}{\tau_E}(E_n - E) \tag{7}$$

$$\frac{dE_M}{dt} = \zeta E(t - \tau_M) \tag{8}$$

Mathematical Model of Reinfection

To model virus re-exposure, the primary infection model was updated to include reactivation of influenza-specific memory CD8$^+$ T cells (E_{IM}) into effector memory cells (E_{EM}) at a nonlinear rate ($\sigma I_1/(K_\sigma + I_1)$) and with decay at d_R per day.

$$\frac{dE_{IM}}{dt} = -\frac{\sigma I_1 E_{IM}}{K_\sigma + I_1} \tag{9}$$

$$\frac{dE_{EM}}{dt} = \frac{\sigma I_1 E_{EM}}{K_\sigma + I_1} - d_R E_{EM} \tag{10}$$

To model clearance of infected cells by effector memory CD8$^+$ T cells, the clearance of infected cells was assumed to occur at equal rates by effector memory CD8$^+$ T cells and newly generated effector cells.

$$\frac{dI_2}{dt} = kI_1 - \delta I_2 - \frac{\delta_E(E + E_{EM})I_2}{K_{\delta_E} + I_2} \tag{11}$$

To model the effect of IFN-γ from memory CD8$^+$ T cells on healthy epithelial cells, we assumed that healthy epithelial cells (T) were removed at a nonlinear rate ($\omega E_{EM}/(K_\omega + E_{EM})$), thereby preventing them from becoming infected.

$$\frac{dT}{dt} = -\beta TV - \frac{\omega E_{EM} T}{K_\omega + E_{EM}} \tag{12}$$

Parameter Quantification

To quantify the model parameters, we fit the model simultaneously to the viral loads and effector and memory CD8$^+$ T cells using a simulated annealing global optimization algorithm as previously described[34,54]. The 95% confidence intervals for the population were obtained through bootstrapping as previously described[34,54]. Parameter uncertainties for each participant were determined by selecting parameter sets that resulted in a cost within 10% of the best-fit cost from a Monte Carlo simulation. Model simulations were implemented in MATLAB or Python.

Estimated parameters in the primary infection model for both the population and individuals included the rates of viral infectivity (β (copies/ml)$^{-1}$ day^{-1}); viral clearance (c day^{-1}); non-specific infected cell clearance (δ day^{-1}); effector CD8$^+$ T cell-mediated infected cell clearance (δ_{E} infected cell (T cell)$^{-1}$ day^{-1}; K_{δ_E} cells); effector CD8$^+$ T cell activation (ξ (infected cell)$^{-1}$ day^{-1}), time delay (τ_{I} days), number of differentiation compartments (n), and time delay (τ_{E} days); and memory CD8$^+$ T cell generation (ζ day^{-1}) and time delay (τ_{M} days). The eclipse phase transition rate was set to k = 6 per day based on prior studies[34,54].

The initial number of healthy epithelial cells ($T(0)$), which also represents the infection size due to all target cells becoming infected within the model, was set to 1 × 10^7 cells for the population but fit for the individuals to estimate differences in infection sizes resulting from different doses. The viral production rate (p (copies/ml)/cells/day) was fit for the population and fixed for each individual. The initial number of eclipse cells ($I_1(0)$) was set to 75 cells, and the initial free virus ($V(0)$) and productively infected cells ($I_2(0)$) were set to 0[34,54]. The initial effector and memory CD8$^+$ T cells ($E(0)$ and $E_M(0)$, respectively) were set to 0 with the baseline values added to the model solution as in our previous studies[34]. For the reinfection models, all model parameters except for those describing memory generation (ζ and τ_{M}) were estimated. The baseline number of influenza-specific memory CD8$^+$ T cells ($E_{MI}(0)$) was assumed to be the number formed during the recorded infection (i.e., value at day 7 – value at day 0).

Clustering Analysis

We performed a principal component analysis (PCA) in Python (scikit-learn.decompose.pca) to cluster individuals with similar host-pathogen interactions. To place parameters on the same scale, parameters were $\log_{10}$-transformed and then normalized using scikit-learn.standardscaler. The optimal clustering was determined using hierarchical clustering[55]

(scipy.cluster.hierarchy.linkage) with Ward's method[56]. The maximum silhouette score[57] from scikit-learn was used to determine the optimal number of clusters.

Modeling Symptom Scores

Our prior work showed that the cumulative area under the curve (CAUC) of infected cells ($I_1 + I_2$) accurately predicts the area of infected tissue, which was correlated to symptoms[34,58]. To estimate the symptom scores recorded by each volunteer, the CAUC was calculated using cumtrapz in MATLAB, with their symptom resolution modeled by a linear decay from the symptom peak[34].

Results

Interindividual Variation in Viral Shedding and CD8$^+$ T cell Patterns

Viral loads in 12 human volunteers who experienced viral shedding for >1 day after being challenged with influenza A/California/04/2009 (H1N1) (Cohort 1) had viral peaks ranging from 5.6 x 10^4 to 2.1 x 10^7 copies/ml, with a population average peak of 2.7 x 10^5 copies/ml on day 2 post-infection[38] (**Figure 1**). The population and most individuals' viral shedding followed a biphasic pattern, with a phase of slower clearance followed by a phase of faster clearance, which was similar to viral shedding patterns observed in murine primary infection models[34,54,58]. Their activated effector CD8$^+$ T cell frequencies increased dramatically during infection, with peak values ranging from 3.0 x 10^5 to 2.4 x 10^7 cells (**Figure 1**), after scaling their relative abundances

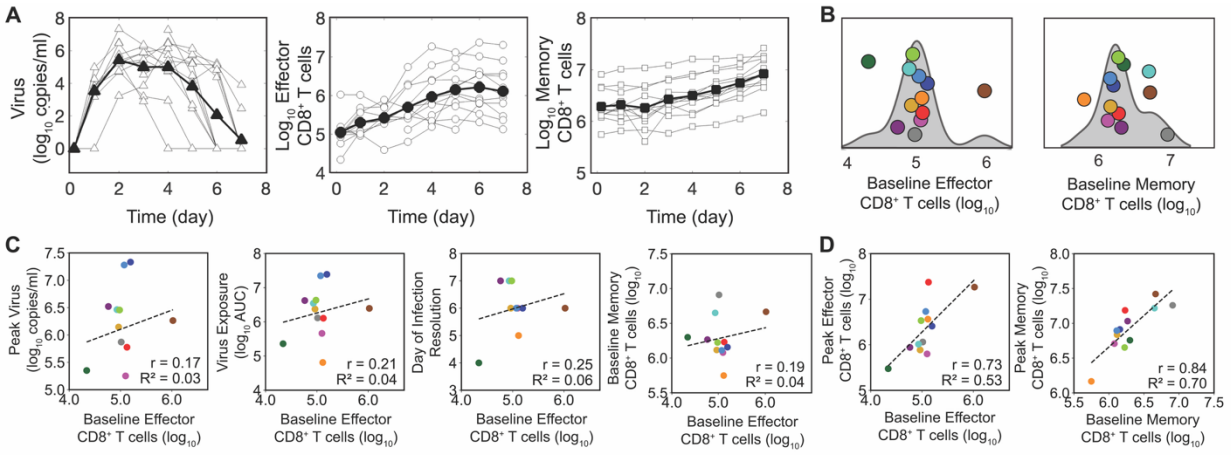

Figure 1. Heterogeneous Viral Shedding and CD8+ T cell Response to Experimental Influenza Challenge in 12 Volunteers. (A) Data from experimental challenge of influenza A virus in 12 volunteers. Population (black markers) and individuals' (open markers) viral shedding (copies/ml) and CD45RA$^+$CD38$^+$CD8$^+$ T cells (effector [CD27$^-$] and memory [CD27$^+$] scaled from abundances). (B) Baseline values of CD8$^+$ T cells were relatively consistent across the cohort. (C) Baseline effector CD8$^+$ T cells were not linearly correlated to the virus peak, virus exposure (AUC), day of resolution, or baseline memory CD8$^+$ T cells. (D) Baseline effector and memory CD8$^+$ T cells were mildly correlated to their respective peak values.

to cell quantities, with the population averaging a 1.16 $\log_{10}$ increase on day 6 post-infection. Their activated memory $CD8^+$ T cells began increasing ~4 days post-infection with individual peaks ranging from 1.5×10^6 to 2.6×10^7 cells, after scaling their relative abundances to cell quantities, with the population averaging a 0.64 $\log_{10}$ increase. Most individuals had relatively similar levels of effector and memory $CD8^+$ T cells at baseline (**Figure 1B**).

We first examined whether baseline effector $CD8^+$ T cells levels could be used to predict viral shedding or T cell patterns using linear correlations. The analysis showed that baseline effector $CD8^+$ T cells were not correlated to virus peak, virus exposure (i.e., area under the curve [AUC]), or day of viral resolution (**Figure 1C**). There were mild correlations between baseline and peak counts for both effector and memory $CD8^+$ T cells ($r = 0.73$ and $r = 0.84$, respectively; **Figure 1D**). However, for effector $CD8^+$ T cells, the correlation was largely skewed by two individuals whose baseline levels were correspondingly above or below most of the cohort, suggesting that baseline levels would likely have minimal predictive power. There were no linear correlations between effector and memory $CD8^+$ T cells or virus and memory $CD8^+$ T cells (**Figure S2**).

Mechanistic Modeling of Individualized Viral Shedding and $CD8^+$ T cell Responses

Because T cell data cannot be directly used to predict the course of infection, we sought to establish the predictability of influenza infections and determine how individuals vary in their rates of viral infectivity, replication, and clearance, in addition to $CD8^+$ T cell expansion, efficacy, and memory generation to create unique infection trajectories. For the population and each influenza-infected individual in Cohort 1, we fit a mechanistic mathematical model (Equations (1)-(8); **Figure 2A**) to their viral load and effector and memory $CD8^+$ T cell data (**Figure 2B-C**; **Table S1**). To avoid skewing the results for those experiencing a primary influenza infection, two of the individuals (IDs 112 and 311) were excluded from this analysis due to their early effector $CD8^+$ T cell response (within one day post-infection), suggestive of pre-existing immunity despite testing negative for influenza-specific antibodies. For the remaining 10 individuals, the resulting model fits accurately captured the observed dynamics, including a biphasic viral decay and heterogeneity in viral loads and $CD8^+$ T cell responses between individuals (**Figure 2**).

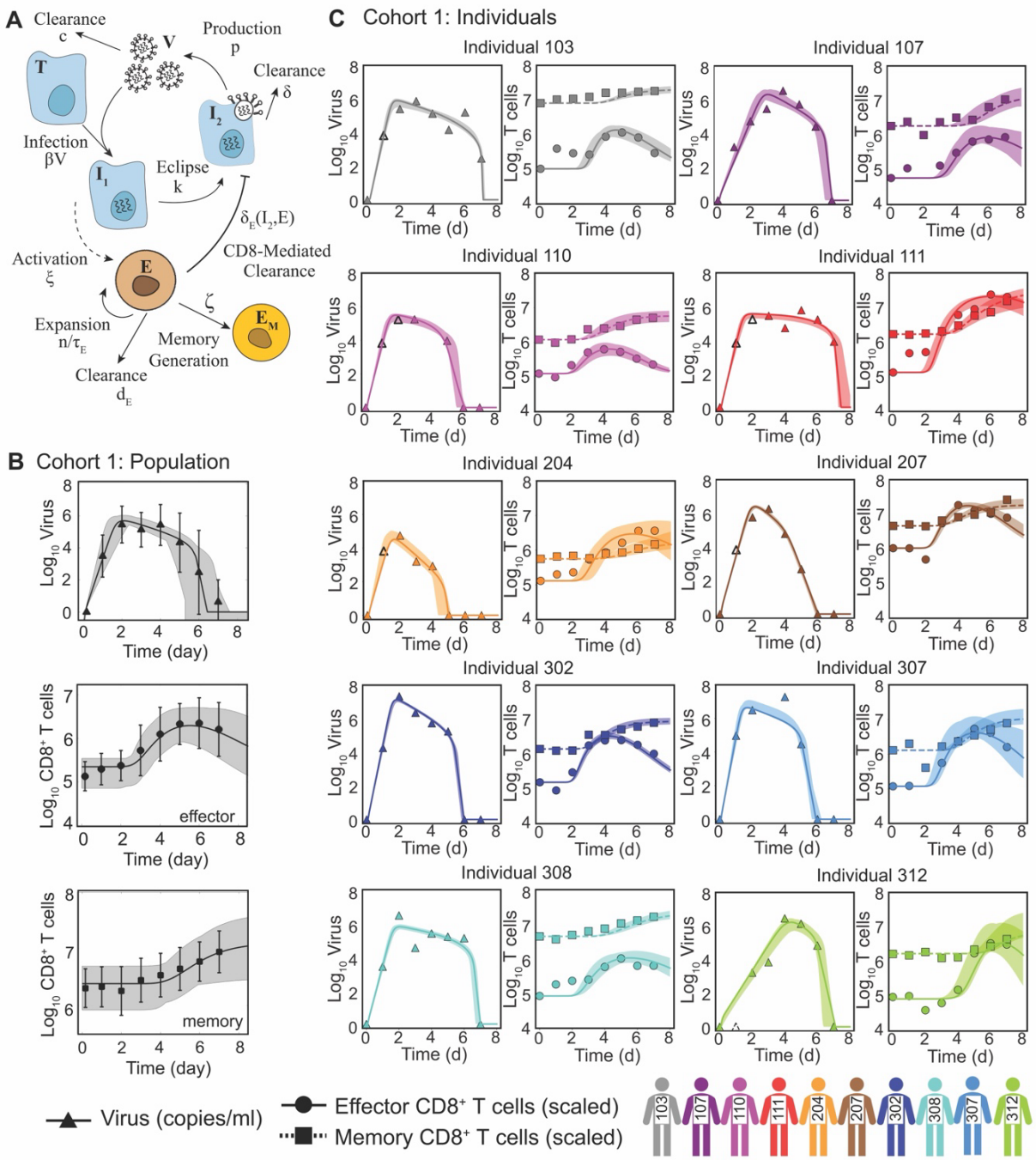

Figure 2. Mechanistic Modeling of Viral Shedding and CD8⁺ T cell Responses in a Cohort of Primary Influenza Infection. (A) Schematic of the mechanistic mathematical model describing human influenza infection in the absence of pre-existing immunity. The model includes clearance by innate mechanisms and cytotoxic effects of $CD8^+$ T cells. (B-C) Population and individual viral shedding and $CD45RA^+CD38^+CD8^+$ T cells (effector [$CD27^-$] and memory [$CD27^+$] scaled from abundances) from Cohort 1 along with the model fits. Open markers indicate imputed viral loads where data was missing. The model captures the biphasic viral load decay in addition to varying timing and magnitudes of T cells.

Multivariate Drivers of Interindividual Heterogeneity

The quantified rates of host-pathogen interactions demonstrated inherent heterogeneity in multiple processes of the infection and the immune response (**Figure 3**; **Figure S3**). The infection size (T_0) was the most prominent difference between individuals (**Figure 3A**), where estimated values ranged between 2.5 x 10^6 and 3.4 x 10^8 cells. From the viral load dynamics alone, there was little indication that the doses and volumes used to infect the volunteers (3.5 x 10^6 $TCID_{50}$ in 250 μl, 7 x 10^6 $TCID_{50}$ in 250 μl, or 7 x 10^6 $TCID_{50}$ in 500 μl) led to distinct infection trajectories or immune responses. However, we previously showed that small differences in viral loads can result in large differences in the amount of the respiratory tract that becomes infected (i.e., infection

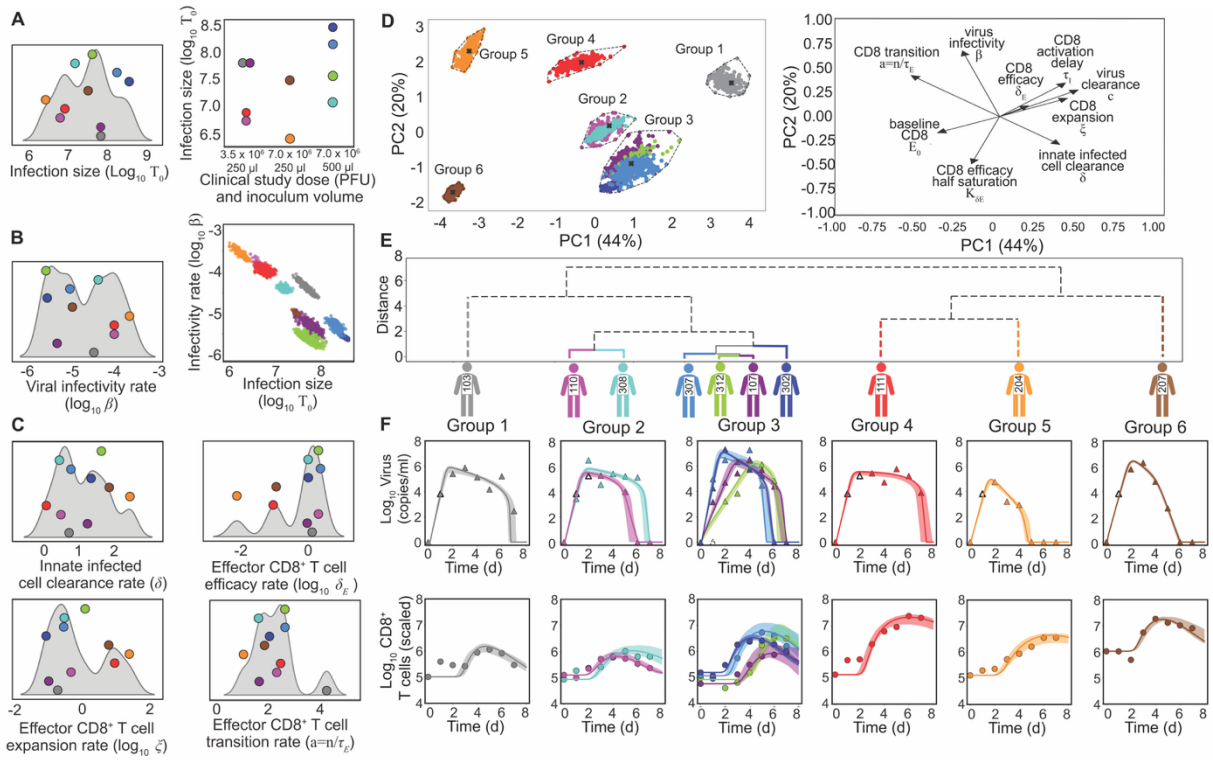

Figure 3. Multivariate Host-Pathogen Interactions Driving Heterogeneous Viral Shedding and CD8⁺ T cell Patterns During Influenza Virus Infection. (A-C) Heterogeneity in the best-fit model parameters for each volunteer infected with influenza A virus. Individuals varied dramatically in their estimated infection sizes (T_0), which aligned with differences in dosing (A), and in their viral infectivity rates (β), which were negatively correlated to the infection size across the population (B). Parameters controlling infected cell clearance by innate (δ) and effector CD8⁺ T cells (δ_E) also varied in addition to effector CD8⁺ T cell expansion ($\xi, a = n/\tau_E$). Parameters not shown are in **Figure S3**. (D) PCA of the individualized parameter sets showing 6 distinct groups identified by hierarchical clustering for the scenario where infection sizes were variable. (E) Dendrogram of the hierarchical clustering, where the number and color of the terminal branches match that of the individual. (F) Corresponding model fits to viral loads (top row; triangles) and scaled effector CD8⁺ T cells (bottom row; circles).

size) in addition to large changes to $CD8^+$ T cell counts[34]. Moreover, there may have been variation in the amount of virus each individual received, which can occur from variation in technique, epithelial cell susceptibility, and/or nasal passage size and structure. The predicted infections sizes captured the different doses and inoculum volumes used in the challenge study, where volunteers receiving 3.5 x 10^6 $TCID_{50}$ in 250 μl (participant IDs 103, 107, 110, and 111) had 0.6 $\log_{10}$ lower infection sizes on average compared to volunteers receiving 7 x 10^6 $TCID_{50}$ in 500 μl (participant IDs 302, 307, 308, and 312) (**Figure 3A**). However, there was variability even within each infection group, possibly indicating inherent differential susceptibility amongst the volunteers.

The infectivity rates (β) also varied significantly between individuals, and there was a notable negative correlation between the estimated infection sizes and the rates of viral infectivity across the population (**Figure 3B**). The individual with the lowest infection size (volunteer ID 204) had the highest innate infected cell clearance rate (δ; **Figure 3C**) and was able to resolve the infection before mounting a $CD8^+$ T cell response. Despite this, their estimated rate of effector $CD8^+$ T cell expansion (ξ) was the highest, but this was coupled with a slower arrival rate ($a = n/\tau_E$), resulting in peak levels several days after infection resolution. The individualized innate infected cell clearance rates (δ), which control the slope of the earlier, slower viral decay phase, varied amongst the other individuals as did other interaction rates, including the rates of effector $CD8^+$ T cell expansion (ξ) and memory $CD8^+$ T cell generation (ζ) (**Figure 3C**). Interestingly, effector $CD8^+$ T cell efficacy (δ_E) was largely similar within the cohort, suggesting that the T cell response is appropriate for most individuals given their infection size. The three individuals with the lowest rates of $CD8^+$ T cell efficacy (δ_E) had the highest $CD8^+$ T cell expansion rates (ξ), signifying a tradeoff such that more cells are required when potency is lower.

Clustering Analysis Revealed Six Distinct Host-Pathogen Patterns

The interindividual variability across multiple processes suggested that multivariate host-pathogen interactions (i.e., combinations of model parameters) were important to investigate to uncover distinct patterns between the influenza-infected individuals. To do this, we performed a principal component analysis (PCA) with hierarchical clustering of the baseline effector $CD8^+$ T cell levels and the rates of infection and immunity that lead to distinct infection trajectories (**Figure 3D-F**). For this analysis, we excluded the differences in the infection sizes (i.e., T_0) because this would reflect epidemiologic variation, while the other rate parameters would be indicative of

inherent biological variability. We also excluded the parameters controlling memory generation to focus on the active response to a primary infection.

Using the first two principal components, which accounted for 44% and 20% of the variance, the 10 volunteers in Cohort 1 separated into six groups (**Figure 3D-F**). Four of the ten volunteers (Group 1 [ID 103], Group 4 [ID 111], Group 5 [ID 204], and Group 6 [ID 207]) were dissimilar from all others in the cohort while the remaining six individuals fell into one of two groups (Group 2 [IDs 110 and 308] and Group 3 [IDs 207, 302, 307, and 312]). Interestingly, most of the volunteers receiving the higher dose and volume clustered together or nearby (Groups 2-3; **Figure 3E**). This analysis reiterated the importance of considering multivariate host-pathogen interactions when interpreting infection dynamics, highlighting that individuals differ from one another in complex and nonuniform ways. It also illustrates that similar host-pathogen interactions can lead to variable viral shedding patterns (e.g., as observed in Group 3), driven by $CD8^+$ T cell responses that are appropriate for each individual's infection.

H1N1 Strain-Dependent Variability

We next sought to identify the cross-cohort variability in viral load dynamics using data from volunteers in Cohort 2, who were infected with a different influenza strain (A/Texas/36/91 (H1N1)) and dose (1×10^5 $TCID_{50}$) than those in Cohort 1. Because the studies for Cohort 2 only reported viral load measurements, we used a reduced viral dynamics model that implicitly describes the efficacy of $CD8^+$ T cells (Equations 1-4 with $\delta(I_2) = \delta_D/(K_\delta + I_2)$). Fitting the model to the population data resulted in a higher rate of virus production (p) for the influenza A/Texas/36/91 strain compared to the influenza A/California/04/2009 strain (0.34 $TCID_{50}$/cell/day versus 0.27 copies/ml/day; **Figure S4; Table S2**). The resulting infection parameters from fitting the model to data for each individual indicated similar infection sizes (T_0; P = 0.21) and overlapping host-pathogen interactions. There were higher average rates of virus infectivity (β; P = 0.002) and infected cell clearance (δ/K_δ; P = 0. 004) for the influenza A/Texas/36/91 strain compared to the influenza A/California/04/2009 strain. These parameters are tightly correlated in this model[34] and may suggest strain-dependent variability in innate- and/or $CD8^+$ T cell-mediated clearance in addition to variability in virus replication. However, overlapping distributions between these rates suggest that the statistical significance may stem from the greater number of individuals in Cohort 2.

Relating Infection Dynamics to Symptoms Highlights Individual Subjectivity

We next investigated whether it was possible to predict symptom scores using the information gained from our model fits. Our prior studies established that the cumulative area under the curve (CAUC) of the predicted infected cell dynamics was an accurate estimate of the infected tissue area, which was related to disease severity[34,58]. Here, we examined whether this same metric could be used to predict human symptoms, which were self-reported and ranged from zero reported symptoms to a peak total score of 17 on a scale of 0 to 51 within Cohort 1, while individuals in Cohort 2 had symptom scores that ranged from 0 to 14 on a scale of 0 to 36 (**Figure 4**).

The results showed good agreement between the CAUC and symptom scores for the population and individuals from both Cohorts (**Figure 4A-C**). To transform the units from the model-predicted values (cells) to symptom scores, we used a scaling factor (α). The average symptom scales were α_1 = 0.52 (range: 0 to 1.3) for Cohort 1 and α_2 = 3.8 (range: 0 to 19.6) for Cohort 2 (**Figure**

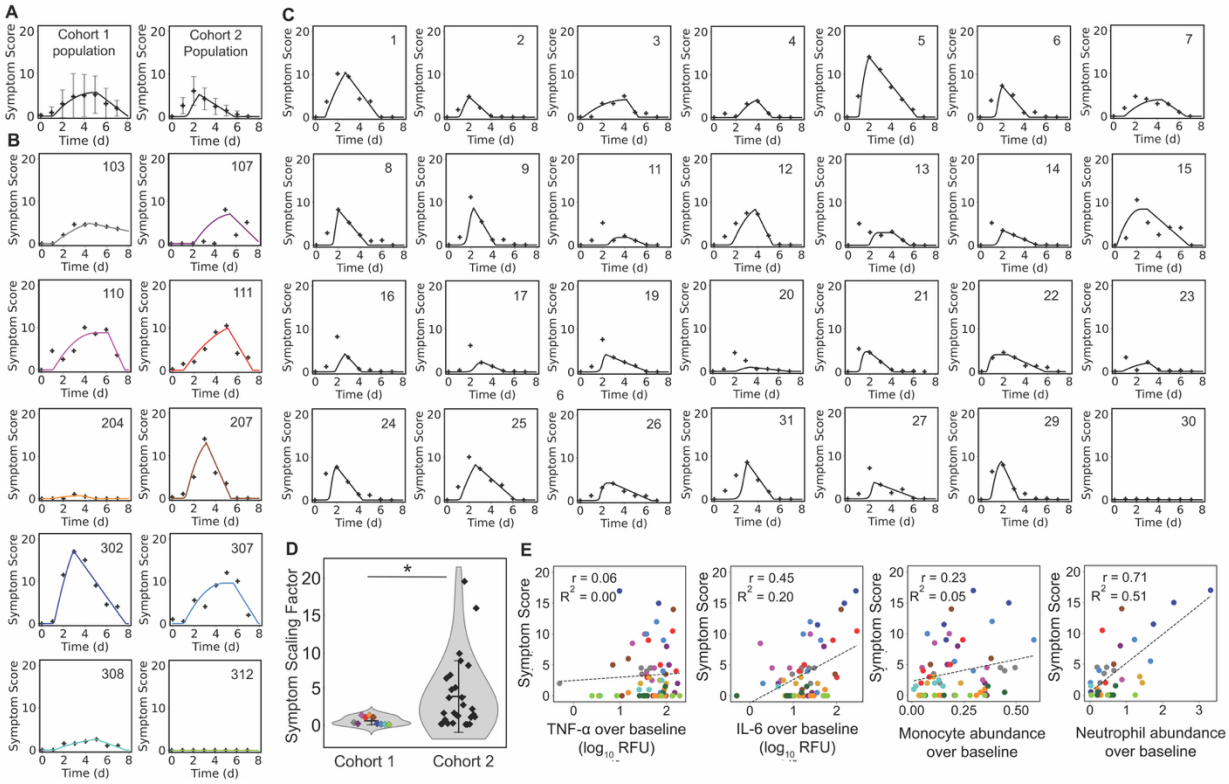

Figure 4. Predicting Symptom Heterogeneity from Infection Dynamics. (A-C) The cumulative area under the curve (CAUC) of model-predicted infected cells dynamics (solid lines) fit to reported symptom scores (markers) for the (A) population (mean ± standard deviation), (B) individuals in Cohort 1, and (C) individuals in Cohort 2. The models fit for each individual in Cohort 2 are in **Figure S4**. (D) Heterogeneity in the estimated scaling factor ($\boldsymbol{\alpha}$) linking the CAUC and symptom score. (E) Linear correlation analysis between symptom scores and TNF-α, IL-6, monocyte abundances, and neutrophil abundances.

4D). Despite a statistically significant difference in mean values (P = 0.001), the extensive overlap between distributions indicates that the effect may lack biological relevance. These results indicate potential subjectivity in the perception of symptomology but do not robustly contribute to viral shedding dynamics. This could be a consequence of variability in other immune processes that relate to symptomology, such as cytokines or innate immune cells. To examine whether symptoms were linearly correlated to variations in innate immunity in the blood, we plotted the symptom scores for Cohort 1 against IL-6 and TNF-α, which are known to cause symptoms, and monocyte and neutrophil frequencies (**Figure 4E**). The were no strong correlations, but there was a mild positive association between symptom scores and neutrophil frequencies (r ~ 0.7).

Individual Variability during Reinfection

We next analyzed two of the individuals in Cohort 1 (IDs 112 and 311) who we suspected had pre-existing T cell immunity despite testing negative for antibodies against the influenza strain. For both individuals, effector $CD8^+$ T cells increased beginning on day 1 post-infection with two peaks of similar magnitude: an early peak at 2-3 days, consistent with a rapid memory response, and a later peak at 5-6 days, resembling the response expected during a primary infection (**Figure 5**). One of the individuals (ID 311) also had lower viral loads and a shorter infection duration compared to the others in the cohort.

To model the possibility that these two individuals were experiencing a reinfection, we updated the primary infection model to include a term for reactivation of memory $CD8^+$ T cells (Equations 9-11). The reinfection model assumes that memory $CD8^+$ T cells reactivate proportionally to newly infected epithelial cells at a nonlinear rate ($\sigma(I_1) = \sigma I_1/[K_\sigma + I_1]$) to become memory effector cells (E_{ME}). Fitting this model to the data from volunteer IDs 112 and 311 captured their viral loads and early increases in effector $CD8^+$ T cells (**Figure 5A**). Memory $CD8^+$ T cell reactivation rates (σ_{112} = 0.34 day^{-1} versus σ_{311} = 0.06 day^{-1}) and half-saturation constants ($K_{\sigma,112}$ = 3.5 x 10^4 cells versus $K_{\sigma,311}$ = 7.4 x 10^3 cells) differed between the two volunteers (**Figure 5B**). $CD8^+$ T cell efficacy was higher for volunteer ID 112 ($\delta_{E,112}$= 8.0 infected cells/T cell/day) than volunteer 311 ($\delta_{E,112}$ = 4.4 infected cells/T cell/day), and both values were marginally above those of the other volunteers (**Figure 5B**), consistent with prior infection. Infection sizes and host-pathogen interactions were consistent with those of other volunteers (**Figure 5B**; **Table S3**), suggesting that key mechanistic features of infection are conserved and, therefore, predictable.

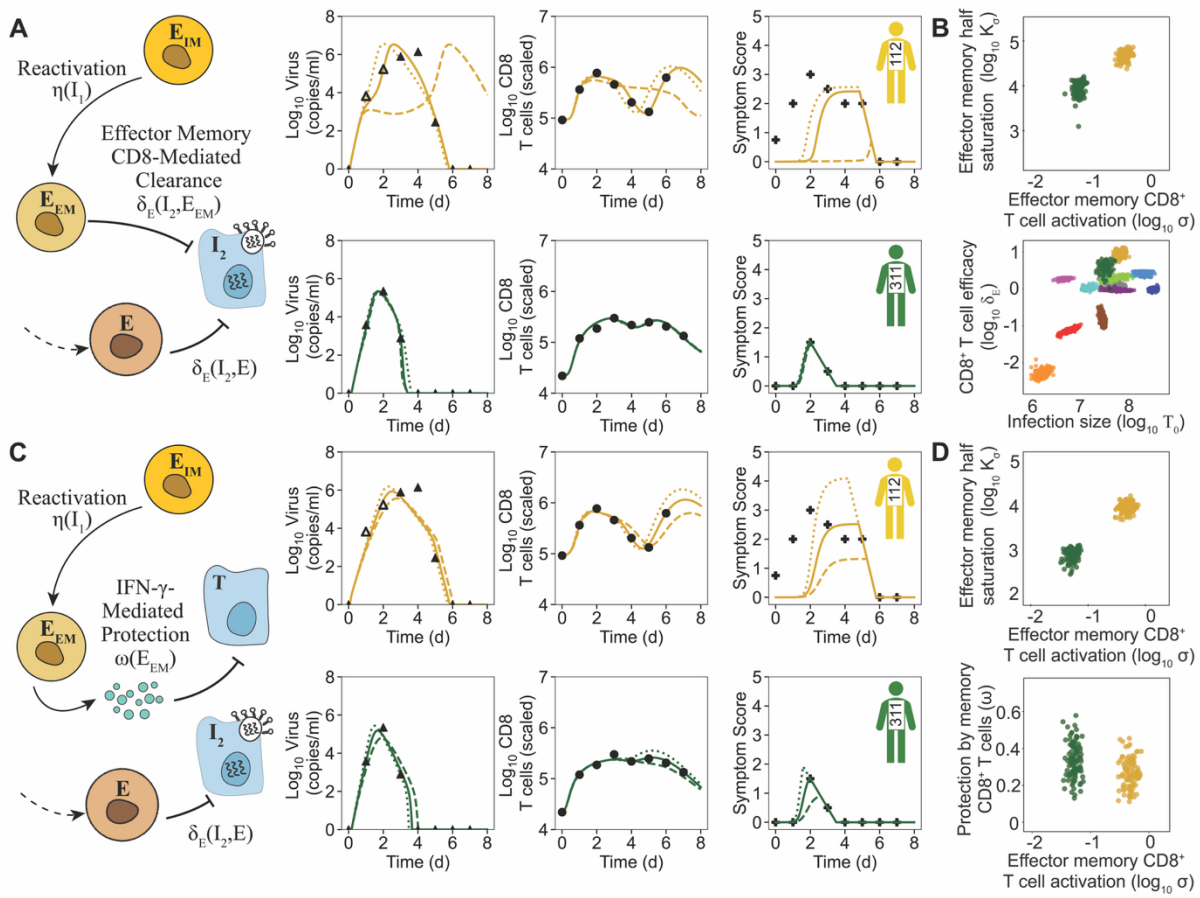

Figure 5. Modeling Mechanisms and Heterogeneity in Memory CD8⁺ T cell Responses during Reinfection. (A) Reinfection model schematic and fits to viral loads (triangles) and effector CD8⁺ T cells (circles) from volunteers 112 (gold) and 311 (green), assuming memory CD8⁺ T cells reactivate ($\boldsymbol{\sigma(I_1)}$) into effector memory cells ($\boldsymbol{E_{EM}}$) and exert cytotoxicity ($\boldsymbol{\delta_E(I_2, E_{EM})}$) at the same rate as recruited CD8⁺ T cells. Modulating efficacy ($\boldsymbol{\delta_E}$) by ±50% altered viral shedding but not symptoms. (B) Reactivation rates differed between volunteers, whereas CD8⁺ T cell efficacy, infection sizes, and other host-pathogen interactions were consistent with the cohort. (C) Alternative model assuming IFN-γ-mediated protection of healthy cells ($\boldsymbol{\omega(E_{EM})}$) fit the data equally well, indicating that cytotoxic and protective effects cannot be distinguished using viral load and T cell data alone. Adjusting protection rates ($\boldsymbol{\omega}$) by ±100% had greater impact on symptoms than on viral loads. (D) Reactivation rates again differed, while protection rates and other parameters were similar to the cohort.

Because IFN-γ secretion by lung-resident CD8⁺ T cells can alter epithelial cell transcription and reduce their susceptibility to infection[59–64], we modeled this effect by allowing healthy cells to become resistant at a nonlinear rate ($\omega(E_{EM}) = \omega E_{EM}/(K_\omega + E_{EM})$; Equation 12). This model fit the data equally well while excluding effector memory CD8⁺ T cell cytotoxicity (**Figure 5C**; **Table S3**), suggesting that the effect of these two mechanisms cannot be separated using viral and T cell data. The estimated memory CD8⁺ T cell reactivation rates (σ_{112} = 0.42 day^{-1} versus σ_{311} = 0.05 day^{-1}) closely matched those obtained from the cytotoxic reinfection model (**Figure 5D**).

However, the half-saturation constants were lower ($K_{\sigma,112}$ = 8.0 x 10^3 cells and $K_{\sigma,311}$ = 8.0 x 10^2 cells), reflecting the smaller number of cells that became infected. The epithelial cell protection parameters were comparable between the two individuals (ω_{112}= 0.26 day^{-1} and ω_{311}= 0.33 day^{-1}; $K_{\omega,112}$= 1.32 x 10^3 cells and $K_{\omega,112}$= 1.85 x 10^2 cells), indicating similar induction of resistance (**Figure 5D**). Other parameters were again generally aligned with those of other cohort members (**Table S3**), reinforcing the consistency and predictability of infection outcomes independent of influenza infection history.

Although simultaneous assessment of the two mechanisms was not possible due to equivalent model fits, two distinctions emerged: the predicted fraction of infected cells and the shape of viral shedding trajectories (**Figure 5**). In the IFN-γ protection model, fewer infected cells increased the symptom scaling factor for volunteer 112 (α_{112} = 1.02 versus 0.29) but had minimal effect for volunteer 311 (α_{311} = 0.52 versus 0.55), with both values remaining within cohort ranges. Modifying the protection rate (ω) had little impact on viral loads but substantially altered symptomology. Increasing memory $CD8^+$ T cell cytotoxicity rates (δ_E) produced distinct viral shedding patterns, with slower early clearance and plateauing before a later peak. Interestingly, this dynamic was evident in volunteers 107, 112, and 312 (**Figures 1 and 5**).

Discussion

Identifying how variations in immunity result in heterogeneous infection dynamics and outcomes to human influenza infection is important to understanding this complicated disease. In addition to having different baseline immune profiles, humans exhibit varying degrees of immunity in response to influenza. Despite T cells being statistically correlated to a decreased risk of infection, our analyses show that this is more nuanced. This partly reflects nonlinear host-pathogen relationships, which complicate direct interpretation of viral shedding and T cell data and increase the likelihood of spurious statistical correlations[37]. Through mechanistic mathematical modeling, we enhanced predictability and data interpretability, revealing that infection landscapes are governed not by single correlates, but by the interplay of viral dose and intrinsic multivariate individuality in viral and host factors, some of which may be clinically unmeasurable.

When accounting for mechanistic linkages and differences in viral dose, several volunteers clustered together despite variation in estimated rates of viral replication and $CD8^+$ T cell responses, indicating that not all heterogeneity is biologically meaningful. Infection trajectories may bifurcate among otherwise similar individuals once key immune or viral processes cross a

critical threshold, particularly at higher infectious doses or in the presence of comorbidities. Identifying where these thresholds occur will be critical for understanding and predicting host-pathogen interactions and for determining the individual-specific points at which T cell responses might shift from protective to immunopathological or confer protection against reinfection. Viral and $CD8^+$ T cells do not seem to vary sufficiently to serve as strong indicators of disease severity. In both human and animal studies, macrophages and neutrophils have instead emerged as potential biomarkers of severe influenza[1,7,8,10–12,15–17,19,22]. For Cohort 1, neutrophil frequencies showed the strongest correlation with symptom scores, although they were not required to predict symptom trajectories. Modeling these cells will be important to better predict divergent outcomes for influenza.

The infection variability resulting from differences in viral doses and infectivity emphasizes the challenge in predicting influenza infections when initial conditions and viral strain are unknown. Beyond transmission route or, in experimental challenges, infection technique, several factors may contribute to smaller initial viral seedings, including enhanced phagocytosis by tissue-resident macrophages and dendritic cells, as well as genetic or functional variation in epithelial cells. This may align with studies that statistically associate higher frequencies of NK cells, monocytes, and $\gamma\delta$ T cells in the blood with increased susceptibility and disease[1–3,8,11,12,15,17,22,23,65], although we caution against overinterpreting such correlations as most studies lack time resolution to identify early deviation points.

Most individuals exhibiting similar rates of T cell efficacy and expansion, even during reinfection, is consistent with the idea that otherwise healthy individuals mount an “appropriate” response for their infection size. This aligns with our earlier murine influenza modeling and T cell depletion experiments, which showed that reducing $CD8^+$ T cells by more than 2 $\log_{10}$ did not alter the rate of virus clearance[34], emphasizing that T cell counts are best interpreted with the help of mechanistic models and in the context of viral loads or other infection characteristics. In those who deviated from this pattern, T cell efficacy was negatively related to expansion rate, suggesting that larger numbers of T cells compensate for reduced per-cell function. In contrast, innate immune clearance of infected cells, which largely determines the slope of viral decline after the peak[66], showed greater variability, likely leading to differences in the timing of T cell responses influenced by early dendritic cell activity.

Host–pathogen interactions during reinfection fell within the range observed for primary infections, indicating that the mechanistic model reliably predicts infection outcomes. Whether the volunteers with rapid T cell responses had immunity specific to the challenge strain or to a related influenza strain remains unclear and may explain why infection and viral shedding still occurred. A similar human challenge study found that nearly all individuals were reinfected one year after initial exposure[41]. Clarifying the roles of distinct $CD8^+$ T cell–mediated mechanisms could help explain these findings, especially since prior infection with unrelated influenza viruses can provide partial protection. In a larger cohort, greater resolution would allow quantification of heterogeneity in $CD8^+$ T cell reactivation and assessment of how baseline memory levels influence outcomes. Reinfection and symptom severity likely vary with waning immunity, exposure history, and strain differences, yet these dynamics appear predictable within the framework of the model.

Predicting symptom dynamics is central to understanding influenza severity. Our mechanistic model links symptoms to the cumulative number of infected cells, consistent with prior mouse studies showing that symptom severity reflects tissue damage[34,58]. It also reproduces earlier findings that small viral load differences can produce large variations in symptom severity and accounts for individuals who shed virus without noticeable symptoms[34]. The relationship between infection dynamics and symptom expression suggests interindividual differences in how tissue-level immunity translates to clinical symptoms. The model underestimated early symptoms in some individuals, likely reflecting systemic responses such as fever rather than respiratory symptoms like coughing[67,68]. Future models incorporating validated representations of innate immune responses should clarify their contribution to protection from symptomatic influenza. Overall, these results highlight the utility of mechanistic modeling for predicting individual outcomes beyond what peripheral immune measures can explain.

These results collectively highlight the importance of understanding host immune responses when interpreting viral loads. Our analyses were limited by the original datasets, which lacked time-resolved measurements and absolute cell counts, constraining the resolution of infection dynamics. Viral loads alone provide little insight into innate immunity or other factors that shape protection and disease severity. In natural infections, where multiple influenza strains circulate and evolve, heterogeneity in dose and viral replication further complicates interpretation. Detailed immune measurements combined with mechanistic modeling are therefore essential to disentangle these complex dynamics.

These findings highlight the power of mechanistic modeling to predict influenza infection dynamics and disease severity, moving beyond single correlates to capture multiparameter viral-host interactions. By focusing on how heterogeneity affects outcomes rather than its underlying causes, models can accommodate variation in human immunity. While questions remain regarding the roles of innate, humoral, and trained immunity, our work demonstrates that mechanistic approaches can substantially improve the predictability of infection outcomes across individuals and populations.

Acknowledgments

This work was supported by the NIH NIAID under award numbers R01AI170115 and R01AI139088 and, in part, thanks to the Canada Research Chair in Computational Immunology with funding from the Canada Research Chairs Program.

References

1. Bodin, J. *et al.* High-dimensional single-cell phenotyping unveils persistent differences in immune cell profiles between severe and moderate seasonal influenza. *Front. Immunol.* **16**, 1576861 (2025).
2. Bongen, E., Vallania, F., Utz, P. J. & Khatri, P. KLRD1-expressing natural killer cells predict influenza susceptibility. *Genome Med* **10**, 45 (2018).
3. Mettelman, R. C. *et al.* Baseline innate and T cell populations are correlates of protection against symptomatic influenza virus infection independent of serology. *Nat Immunol* **24**, 1511–1526 (2023).
4. Allen, E. K. *et al.* SNP-mediated disruption of CTCF binding at the IFITM3 promoter is associated with risk of severe influenza in humans. *Nat Med* **23**, 975–983 (2017).
5. Choreño-Parra, J. A. *et al.* CXCL17 Is a Specific Diagnostic Biomarker for Severe Pandemic Influenza A(H1N1) That Predicts Poor Clinical Outcome. *Front. Immunol.* **12**, 633297 (2021).
6. Fiore-Gartland, A. *et al.* Cytokine Profiles of Severe Influenza Virus-Related Complications in Children. *Front. Immunol.* **8**, 1423 (2017).
7. Parnell, G. P. *et al.* A distinct influenza infection signature in the blood transcriptome of patients with severe community-acquired pneumonia. *Crit Care* **16**, R157 (2012).
8. MOSAIC Investigators *et al.* Progression of whole-blood transcriptional signatures from interferon-induced to neutrophil-associated patterns in severe influenza. *Nat Immunol* **19**, 625–635 (2018).
9. Parnell, G. *et al.* Aberrant Cell Cycle and Apoptotic Changes Characterise Severe Influenza A Infection – A Meta-Analysis of Genomic Signatures in Circulating Leukocytes. *PLoS ONE* **6**, e17186 (2011).
10. Tang, B. M. *et al.* Neutrophils-related host factors associated with severe disease and fatality in patients with influenza infection. *Nat Commun* **10**, 3422 (2019).

11. Wong, S.-S. *et al.* Severe Influenza Is Characterized by Prolonged Immune Activation: Results From the SHIVERS Cohort Study. *The Journal of Infectious Diseases* **217**, 245–256 (2018).
12. Cole, S. L. *et al.* M1-like monocytes are a major immunological determinant of severity in previously healthy adults with life-threatening influenza. *JCI Insight* **2**, e91868 (2017).
13. Jha, A. *et al.* Patterns of systemic and local inflammation in patients with asthma hospitalised with influenza. *Eur Respir J* **54**, 1900949 (2019).
14. The GenISIS Investigators *et al.* IFITM3 restricts the morbidity and mortality associated with influenza. *Nature* **484**, 519–523 (2012).
15. Oshansky, C. M. *et al.* Mucosal Immune Responses Predict Clinical Outcomes during Influenza Infection Independently of Age and Viral Load. *Am J Respir Crit Care Med* **189**, 449–462 (2013).
16. Bongen, E. *et al.* Sex Differences in the Blood Transcriptome Identify Robust Changes in Immune Cell Proportions with Aging and Influenza Infection. *Cell Reports* **29**, 1961-1973.e4 (2019).
17. Zhai, Y. *et al.* Host Transcriptional Response to Influenza and Other Acute Respiratory Viral Infections – A Prospective Cohort Study. *PLoS Pathog* **11**, e1004869 (2015).
18. Woods, C. W. *et al.* A Host Transcriptional Signature for Presymptomatic Detection of Infection in Humans Exposed to Influenza H1N1 or H3N2. *PLoS ONE* **8**, e52198 (2013).
19. Schughart, K. *et al.* Host response to influenza infections in human blood: association of influenza severity with host genetics and transcriptomic response. *Front. Immunol.* **15**, 1385362 (2024).
20. Paterson, S. *et al.* Innate-like Gene Expression of Lung-Resident Memory $CD8^+$ T Cells during Experimental Human Influenza: A Clinical Study. *Am J Respir Crit Care Med* **204**, 826–841 (2021).

21. Wilkinson, T. M. *et al.* Preexisting influenza-specific CD4+ T cells correlate with disease protection against influenza challenge in humans. *Nat Med* **18**, 274–280 (2012).
22. O'Neill, M. B. *et al.* Single-Cell and Bulk RNA-Sequencing Reveal Differences in Monocyte Susceptibility to Influenza A Virus Infection Between Africans and Europeans. *Front. Immunol.* **12**, 768189 (2021).
23. Savic, M. *et al.* Distinct T and NK cell populations may serve as immune correlates of protection against symptomatic pandemic influenza A(H1N1) virus infection during pregnancy. *PLoS ONE* **12**, e0188055 (2017).
24. Souquette, A. & Thomas, P. G. Variation in the basal immune state and implications for disease. *eLife* **13**, e90091 (2024).
25. HIPC-CHI Signatures Project Team *et al.* Multicohort analysis reveals baseline transcriptional predictors of influenza vaccination responses. *Sci. Immunol.* **2**, eaal4656 (2017).
26. The Milieu Intérieur Consortium *et al.* Natural variation in the parameters of innate immune cells is preferentially driven by genetic factors. *Nat Immunol* **19**, 302–314 (2018).
27. Liston, A., Humblet-Baron, S., Duffy, D. & Goris, A. Human immune diversity: from evolution to modernity. *Nat Immunol* **22**, 1479–1489 (2021).
28. Sparks, R. *et al.* A unified metric of human immune health. *Nat Med* **30**, 2461–2472 (2024).
29. Kotliarov, Y. *et al.* Broad immune activation underlies shared set point signatures for vaccine responsiveness in healthy individuals and disease activity in patients with lupus. *Nat Med* **26**, 618–629 (2020).
30. Hensen, L. *et al.* CD8+ T cell landscape in Indigenous and non-Indigenous people restricted by influenza mortality-associated HLA-A*24:02 allomorph. *Nat Commun* **12**, 2931 (2021).
31. Furman, D. *et al.* Cytomegalovirus infection enhances the immune response to influenza. *Sci. Transl. Med.* **7**, 281ra43-281ra43 (2015).

32. Elias, G. *et al.* Altered CD4 $^{+}$ T cell immunity in nurses occupationally exposed to viral pathogens. *Clin Exp Immunol* **194**, 192–204 (2018).

33. Pronier, C. *et al.* Respiratory Influenza viral load as a marker of poor prognosis in patients with severe symptoms. *Journal of Clinical Virology* **136**, 104761 (2021).

34. Myers, M. A. *et al.* Dynamically linking influenza virus infection kinetics, lung injury, inflammation, and disease severity. *eLife* **10**, e68864 (2021).

35. McKay, B. *et al.* Associations Between Relative Viral Load at Diagnosis and Influenza A Symptoms and Recovery. *Open Forum Infectious Diseases* **7**, ofaa494 (2020).

36. Lalueza, A. *et al.* Influence of viral load in the outcome of hospitalized patients with influenza virus infection. *Eur J Clin Microbiol Infect Dis* **38**, 667–673 (2019).

37. Smith, A. M. Decoding immune kinetics: unveiling secrets using custom-built mathematical models. *Nat Methods* **21**, 744–747 (2024).

38. Rahil, Z. *et al.* Landscape of coordinated immune responses to H1N1 challenge in humans. *J Clin Invest* **130**, 5800–5816 (2020).

39. Canini, L., Woolhouse, M. E. J., Maines, T. R. & Carrat, F. Heterogeneous shedding of influenza by human subjects and its implications for epidemiology and control. *Scientific Reports 2016 6:1* **6**, 1–9 (2016).

40. Memoli, M. J. *et al.* Validation of the Wild-type Influenza A Human Challenge Model H1N1pdMIST: An A(H1N1)pdm09 Dose-Finding Investigational New Drug Study. *Clinical Infectious Diseases* **60**, 693–702 (2015).

41. Memoli, M. J. *et al.* Influenza A Reinfection in Sequential Human Challenge: Implications for Protective Immunity and “Universal” Vaccine Development. *Clinical Infectious Diseases* **70**, 748–753 (2020).

42. Walters, K.-A. *et al.* Nasal and systemic immune responses correlate with viral shedding after influenza challenge in people with complex preexisting immunity. *Sci. Transl. Med.* **17**, eadt1452 (2025).

43. Hayden, F. G. *et al.* Local and systemic cytokine responses during experimental human influenza A virus infection. Relation to symptom formation and host defense. *Journal of Clinical Investigation* **101**, 643–649 (1998).

44. Hayden, F. G. *et al.* Use of the Oral Neuraminidase Inhibitor Oseltamivir in Experimental Human Influenza: Randomized Controlled Trials for Prevention and Treatment. *JAMA* **282**, 1240 (1999).

45. Hayden, F. G. *et al.* Oral LY217896 for prevention of experimental influenza A virus infection and illness in humans. *Antimicrob Agents Chemother* **38**, 1178–1181 (1994).

46. Killingley, B. *et al.* Use of a Human Influenza Challenge Model to Assess Person-to-Person Transmission: Proof-of-Concept Study. *The Journal of Infectious Diseases* **205**, 35–43 (2012).

47. Han, A. *et al.* Using the Influenza Patient-reported Outcome (FLU-PRO) diary to evaluate symptoms of influenza viral infection in a healthy human challenge model. *BMC Infect Dis* **18**, 353 (2018).

48. Calfee, D. P., Peng, A. W., Cass, L. M., Lobo, M. & Hayden, F. G. Safety and Efficacy of Intravenous Zanamivir in Preventing Experimental Human Influenza A Virus Infection. *Antimicrob Agents Chemother* **43**, 1616–1620 (1999).

49. Fritz, R. S. *et al.* Nasal Cytokine and Chemokine Responses in Experimental Influenza A Virus Infection: Results of a Placebo-Controlled Trial of Intravenous Zanamivir Treatment. *J INFECT DIS* **180**, 586–593 (1999).

50. Skoner, D. P., Gentile, D. A., Patel, A. & Doyle, W. J. Evidence for Cytokine Mediation of Disease Expression in Adults Experimentally Infected with Influenza A Virus. *J INFECT DIS* **180**, 10–14 (1999).

51. Huang, Y. *et al.* Temporal Dynamics of Host Molecular Responses Differentiate Symptomatic and Asymptomatic Influenza A Infection. *PLoS Genet* **7**, e1002234 (2011).

52. McClain, M. T. *et al.* Longitudinal analysis of leukocyte differentials in peripheral blood of patients with acute respiratory viral infections. *Journal of Clinical Virology* **58**, 689–695 (2013).

53. Lim, J. J. *et al.* Phase 2 Randomized Trial of the Safety and Efficacy of MHAA4549A, a Broadly Neutralizing Monoclonal Antibody, in a Human Influenza A Virus Challenge Model. *Antimicrob Agents Chemother* **61**, (2017).

54. Smith, A. P., Moquin, D. J., Bernhauerova, V. & Smith, A. M. Influenza Virus Infection Model With Density Dependence Supports Biphasic Viral Decay. *Front. Microbiol.* **9**, (2018).

55. Murtagh, F. & Contreras, P. Algorithms for hierarchical clustering: an overview, II. *WIREs Data Mining and Knowledge Discovery* **7**, e1219 (2017).

56. Vijaya, Sharma, S. & Batra, N. Comparative Study of Single Linkage, Complete Linkage, and Ward Method of Agglomerative Clustering. in *2019 International Conference on Machine Learning, Big Data, Cloud and Parallel Computing (COMITCon)* 568–573 (2019). doi:10.1109/COMITCon.2019.8862232.

57. Shahapure, K. R. & Nicholas, C. Cluster Quality Analysis Using Silhouette Score. in *2020 IEEE 7th International Conference on Data Science and Advanced Analytics (DSAA)* 747–748 (2020). doi:10.1109/DSAA49011.2020.00096.

58. Smith, A. P. *et al.* Increased virus dissemination leads to enhanced lung injury but not inflammation during influenza-associated secondary bacterial infection. *FEMS Microbes* **3**, xtac022 (2022).

59. Uddbäck, I. *et al.* Prevention of respiratory virus transmission by resident memory CD8+ T cells. *Nature* **626**, 392–400 (2024).

60. Bot, A., Bot, S. & Bona, C. A. Protective Role of Gamma Interferon during the Recall Response to Influenza Virus. *J Virol* **72**, 6637–6645 (1998).

61. McMaster, S. R., Wilson, J. J., Wang, H. & Kohlmeier, J. E. Airway-Resident Memory CD8 T Cells Provide Antigen-Specific Protection against Respiratory Virus Challenge through Rapid IFN-γ Production. *The Journal of Immunology* **195**, 203–209 (2015).
62. Fong, C. H.-Y. *et al.* Interferon-gamma inhibits influenza A virus cellular attachment by reducing sialic acid cluster size. *iScience* **25**, 104037 (2022).
63. Bukreyev, A., Whitehead, S. S., Bukreyeva, N., Murphy, B. R. & Collins, P. L. Interferon γ expressed by a recombinant respiratory syncytial virus attenuates virus replication in mice without compromising immunogenicity. *Proc. Natl. Acad. Sci. U.S.A.* **96**, 2367–2372 (1999).
64. Hilligan, K. L. *et al.* Bacterial-induced or passively administered interferon gamma conditions the lung for early control of SARS-CoV-2. *Nat Commun* **14**, 8229 (2023).
65. Scharenberg, M. *et al.* Influenza A Virus Infection Induces Hyperresponsiveness in Human Lung Tissue-Resident and Peripheral Blood NK Cells. *Front. Immunol.* **10**, 1116 (2019).
66. Smith, A. M., Adler, F. R. & Perelson, A. S. An accurate two-phase approximate solution to an acute viral infection model. *Journal of Mathematical Biology* **60**, 711–726 (2010).
67. Eccles, R. Understanding the symptoms of the common cold and influenza. *The Lancet Infectious Diseases* **5**, 718–725 (2005).
68. Lee, C.-S. & Lee, J.-H. Dynamics of clinical symptoms in patients with pandemic influenza A (H1N1). *Clinical Microbiology and Infection* **16**, 389–390 (2010).